SUPPORTING INFORMATION

Influence of Ge Substitution on the Structure and Optical Properties of $Cu_2ZnSn_{1-x}Ge_xS_4$ Photovoltaic Materials

Amit Bhattacharya[1], Vidyanshu Mishra[1], Victor V. Terskikh[2], Arthur Mar[1]* and Vladimir K. Michaelis[1]*

1. Department of Chemistry, University of Alberta, Edmonton, Alberta, Canada T6G 2G2

2. Metrology, National Research Council Canada, Ottawa, Ontario, Canada K1A 0R6

NMR Parameters

NMR signals are characterized by two types of tensor quantities:

(a) Chemical shift anisotropy (CSA):

- The position is defined by the *isotropic chemical shift*, $\delta_{\mathrm{iso}} = \frac{1}{3}(\delta_{11}+\delta_{22}+\delta_{33})$, where $\delta_{11} \geq \delta_{22} \geq \delta_{33}$.
- The breadth is defined by the *span*, $\Omega = \delta_{11} - \delta_{33}$.
- The shape is defined by the *skew*, $\kappa = 3(\delta_{22} - \delta_{\mathrm{iso}})/\Omega$.

(b) Quadrupolar interactions for nuclei with $I > ½$:

- The strength of the interaction between a nucleus and the surrounding electric field gradient (EFG) is defined by the *nuclear quadrupole coupling constant*, $C_Q = eQV_{zz}/h$, where e is the elementary charge, Q is the quadrupolar moment of the nucleus, V_{zz} is the largest principal component of the EFG, and h is Planck's constant.
- The symmetry of the EFG tensor is defined by the *asymmetry parameter*, $\eta = (V_{xx} - V_{yy})/V_{zz}$, where $|V_{xx}| \leq |V_{yy}| \leq |V_{zz}|$.

Table S1. Experimental Conditions for Acquisition of NMR Spectra of $Cu_2ZnSn_{1-x}Ge_xS_4$

	^{65}Cu	^{67}Zn	^{119}Sn	^{73}Ge
conditions	non-spinning	non-spinning	non-spinning	non-spinning
B_0 (T)	7.05, 11.75, 21.1	21.1	11.75	21.1
pulse sequence	wideline quadrupolar echo[a]	wideline quadrupolar echo	Hahn echo	Bloch
π/2 pulse (μs)	1	3	4	4
$\gamma B_1/2\pi$ (kHz)	125	28	62.5	12.5
τ (μs)	50	50	30	—
recycle delay (s)	2	5	50–100	5
rotor diameter (mm)	4	4	4	7
co-added transients	1024–8048	15360	1024–2048	8192
	^{63}Cu	^{67}Zn	^{119}Sn	^{73}Ge
conditions	MAS ($\omega_r/2\pi$ = 62.5 kHz)	MAS ($\omega_r/2\pi$ = 10 kHz)	MAS ($\omega_r/2\pi$ = 14 kHz)	MAS ($\omega_r/2\pi$ = 5 kHz)
B_0 (T)	21.1	21.1	7.05	21.1
pulse sequence	wideline quadrupolar echo	Bloch	Hahn echo	Bloch
π/2 pulse (μs)	1	3	4	4
$\gamma B_1/2\pi$ (kHz)	125	27.8	62.5	12.5
τ (μs)	15	—	67.4	—
recycle delay (s)	2	2–5	50–150	2–5
rotor diameter (mm)	1.3	4	4	7
co-added transients	3072–4096	32768	1024–5120	1024–16384

[a] Wide-line quadrupolar echo implies a ($\theta - \tau - \theta - \tau$–acquire) experiment. θ refers to 90° solid pulse with the pulse lengths p1 = p2. See Bodart, P.R., Amoureux, J.P., Dumazy, Y. and Lefort, R. **2000**, Molecular Physics, 98 (19), 1545 and Dumazy, Y., Amoureux, J.P. and Fernandez, C., 2010, Molecular Physics, 90(6), 959

[b]Hahn echo implies a ($\theta - \tau - 2\theta - \tau$–acquire) experiment. θ refers to 90° nutation angle and the pulse length, p2 = 2×p1; p1 is the 90° pulse.

Table S2. Nuclear Larmor frequencies of $^{63/65}$Cu, ^{67}Zn, ^{73}Ge and ^{119}Sn nuclei at the external magnetic field used.

Nucleus	Larmor frequency (MHz) at 7.05 T	Larmor frequency (MHz) at 11.75 T	Larmor frequency (MHz) at 21.1 T
$^{63/65}$Cu	85.25 (^{65}Cu)	142.05 (^{65}Cu)	238.67(^{63}Cu) / 255.67 (^{65}Cu)
^{67}Zn	-	-	56.32
^{73}Ge	-	-	31.39
^{119}Sn	111.90	149.21	-

Table S3. EDX Analyses (mol %) for $Cu_2ZnSn_{1-x}Ge_xS_4$ Samples [a]

x	composition	Cu	Zn	Sn	Ge	S
0	Cu_2ZnSnS_4	26	11	13	0	51
	(nominal)	25	12	13	0	50
0.05	$Cu_2ZnSn_{0.95}Ge_{0.05}S_4$	23	11	13	1	52
	(nominal)	25	12	12	1	50
0.20	$Cu_2ZnSn_{0.80}Ge_{0.20}S_4$	24	10	11	2	53
	(nominal)	25	12	10	3	50
0.40	$Cu_2ZnSn_{0.60}Ge_{0.40}S_4$	24	12	8	5	51
	(nominal)	25	12	8	5	50
0.60	$Cu_2ZnSn_{0.40}Ge_{0.60}S_4$	25	13	5	7	50
	(nominal)	25	12	5	8	50
0.80	$Cu_2ZnSn_{0.20}Ge_{0.80}S_4$	24	12	3	10	51
	(nominal)	25	12	3	10	50
1.00	Cu_2ZnGeS_4	25	12	0	12	51
	(nominal)	25	12	0	13	50

[a] Experimental compositions are shown on first line and expected compositions on second line. Estimated uncertainties are 2% for each element.

Table S4. Cell Parameters for $Cu_2ZnSn_{1-x}Ge_xS_4$. [a]

x	compound	*a* (Å)	*c* (Å)	*V* (Å^3)	η (*c*/2*a* ratio)
0	Cu_2ZnSnS_4	5.4356(3)	10.8354(1)	320.14(2)	0.997
0.05	$Cu_2ZnSn_{0.95}Ge_{0.05}S_4$	5.4294(1)	10.8239(1)	319.08(1)	0.997
0.20	$Cu_2ZnSn_{0.80}Ge_{0.20}S_4$	5.4167(1)	10.7758(1)	316.17(1)	0.995
0.40	$Cu_2ZnSn_{0.60}Ge_{0.40}S_4$	5.3987(2)	10.7128(5)	312.23(2)	0.992
0.60	$Cu_2ZnSn_{0.40}Ge_{0.60}S_4$	5.3754(1)	10.6414(3)	307.48(1)	0.989
0.80	$Cu_2ZnSn_{0.20}Ge_{0.80}S_4$	5.3641(1)	10.5855(1)	304.58(1)	0.987
1.00	Cu_2ZnGeS_4	5.3449(1)	10.5137(1)	300.35(1)	0.983

[a] Refined from powder XRD patterns. Standard uncertainties are shown in parentheses.

Table S5. Atomic Coordinates for Cu_2ZnSnS_4 and Cu_2ZnGeS_4.

atom	Wyckoff position	*x*	*y*	*z*
Cu_2ZnSnS_4 ($I\bar{4}$)				
Cu1	2*c*	0	½	¼
Cu2	2*a*	0	0	0
Zn	2*d*	0	½	¾
Sn	2*b*	0	0	½
S	8*g*	0.2469(4)	0.2524(4)	0.1274(3)
Cu_2ZnGeS_4 ($I\bar{4}$)				
Cu1	2*c*	0	½	¼
Cu2	2*a*	0	0	0
Zn	2*d*	0	½	¾
Ge	2*b*	0	0	½
S	8*g*	0.2601(14)	0.244(4)	0.1217(1)

Table S6. Calculations of the tetragonal angular variance (σ^2) for Cu_2ZnSnS_4 and Cu_2ZnGeS_4 [a]

[a] $\sigma^2 = \frac{1}{5}\sum_{i=1}^{6}(\theta_i - 109.47°)^2$; where θ_i pertains to ∠S-Cu-S angles.

Wyckoff position	Angle A (°)	Angle B (°)	C [$(\theta_i - 109.47°)^2$ for A]	D [$(\theta_i - 109.47°)^2$ for B]	σ^2 [(4×C+2×D)/5] in ($°^2$)
Cu_2ZnSnS_4					
2*c* (Cu1)	109.2 (×4)	110.1 (×2)	0.07	0.39	0.2
2*a* (Cu2)	109.9(×4)	108.5 (×2)	0.18	0.94	0.5
Cu_2ZnGeS_4					
2*c* (Cu1)	108.1 (×2)	112.3 (×4)	1.77	0.45	1.6
2*a* (Cu2)	110.8 (×2)	108.8 (×4)	1.88	8.01	4.7

Table S7. Comparison of Experimental and DFT-Calculated NMR Parameters for Cu_2ZnSnS_4 and Cu_2ZnGeS_4.[a]

	Cu_2ZnSnS_4		Cu_2ZnGeS_4		
	experimental	calculated	experimental	calculated (model A)	calculated (model C)
^{65}Cu parameters					
Ω (ppm)	272 (2*a*), 117 (2*c*)	284 (2*a*), 136 (2*c*)	150 (2*a*), 83 (2*c*)	176 (2*a*), 190 (2*c*)	185
κ	+1 (2*a*), –1 (2*c*)	+1 (2*a*), –1 (2*c*)	–1 (2*a*), –1 (2*c*)	+1 (2*a*), –1 (2*c*)	–1
C_Q (MHz)	6.5 (2*a*), 1.5 (2*c*)	7.1 (2*a*), 3.6 (2*c*)	15.2 (2*a*), 4.3 (2*c*)	15.5 (2*a*), 4.2 (2*c*)	8.2
η	0 (2*a*), 0 (2*c*)	0 (2*a*), 0 (2*c*)	0 (2*a*), 0 (2*c*)	0 (2*a*), 0 (2*c*)	0
^{67}Zn parameters					
Ω (ppm)	29	34	— [b]	15	17
κ	–0.5	–1	— [b]	+1	–1
C_Q (MHz)	0.9	1.8	2.8	5.1	7.4
η	0	0	0.2	0	0
^{119}Sn parameters					
Ω (ppm)	32	39			
κ	–0.4	–1			
^{73}Ge parameters					
Ω (ppm)			14 [b]	26	39
κ			–1 [b]	–1	+1
C_Q (MHz)			0.3	0.3	1.8
η			0.0	0	0

[a] Uncertainties are ±5 ppm for Ω, ±0.05 for κ, ±0.1 MHz for C_Q, and ±0.1 for η. [b] Ω and κ do not noticeably improve the fittings.

Table S8. ^{65}Cu NMR Parameters for $Cu_2ZnSn_{0.8}Ge_{0.2}S_4$ [a]

	δ_{iso} (ppm)	Ω (ppm)	κ	C_Q (MHz)
2*a*_1	761	255	+1	7.5
2*a*_2	720	220	+1	11.8
2*a*_3	690	132	–1	16.5
2*c*_1	795	101	–1	1.5
2*c*_2	805	99	–1	2.6
2*c*_3	780	81	–1	4.4

[a] The labels 1, 2, 3 refer to C_Q values in ascending order for 2*a* and 2*c* sites.

Table S9. Chemical Shifts and Linewidths for ^{119}Sn and ^{73}Ge MAS NMR Spectra for $Cu_2ZnSn_{1-x}Ge_xS_4$

		^{119}Sn		^{73}Ge	
x	compound	δ_{iso} (ppm)	FWHM (Hz)	δ_{cgs} (ppm)	FWHM (Hz)
0	Cu_2ZnSnS_4	121.5	795		
0.05	$Cu_2ZnSn_{0.95}Ge_{0.05}S_4$	–119.8	919	21.2	280
0.20	$Cu_2ZnSn_{0.80}Ge_{0.20}S_4$	–118.1	1252	21.6	195
0.40	$Cu_2ZnSn_{0.60}Ge_{0.40}S_4$	–112.1	1080	23.4	488
0.60	$Cu_2ZnSn_{0.40}Ge_{0.60}S_4$	–111.4	2254	23.1	236
0.80	$Cu_2ZnSn_{0.20}Ge_{0.80}S_4$	–103.2	1199	26.3	151
1.00	Cu_2ZnGeS_4			28.5	95

Table S10. Isotropic Chemical Shifts and Centre-of-Gravity Shifts of ^{67}Zn MAS NMR Spectra for $Cu_2ZnSn_{1-x}Ge_xS_4$

x	compound	δ_{iso} (ppm)	δ_{cgs} (ppm)
0	Cu_2ZnSnS_4	361	359
0.05	$Cu_2ZnSn_{0.95}Ge_{0.05}S_4$		361
0.20	$Cu_2ZnSn_{0.80}Ge_{0.20}S_4$		368
0.40	$Cu_2ZnSn_{0.60}Ge_{0.40}S_4$		382
0.60	$Cu_2ZnSn_{0.40}Ge_{0.60}S_4$		378
0.80	$Cu_2ZnSn_{0.20}Ge_{0.80}S_4$		367
1.00	Cu_2ZnGeS_4	358	343

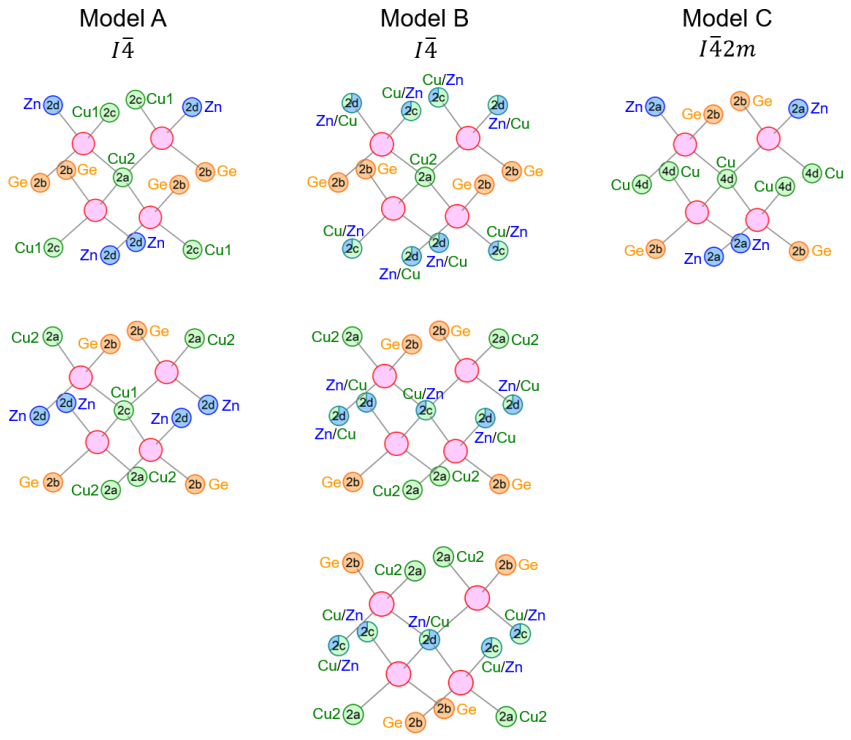

Figure S1. Local environments around Cu atoms in three structural models of Cu_2ZnGeS_4.

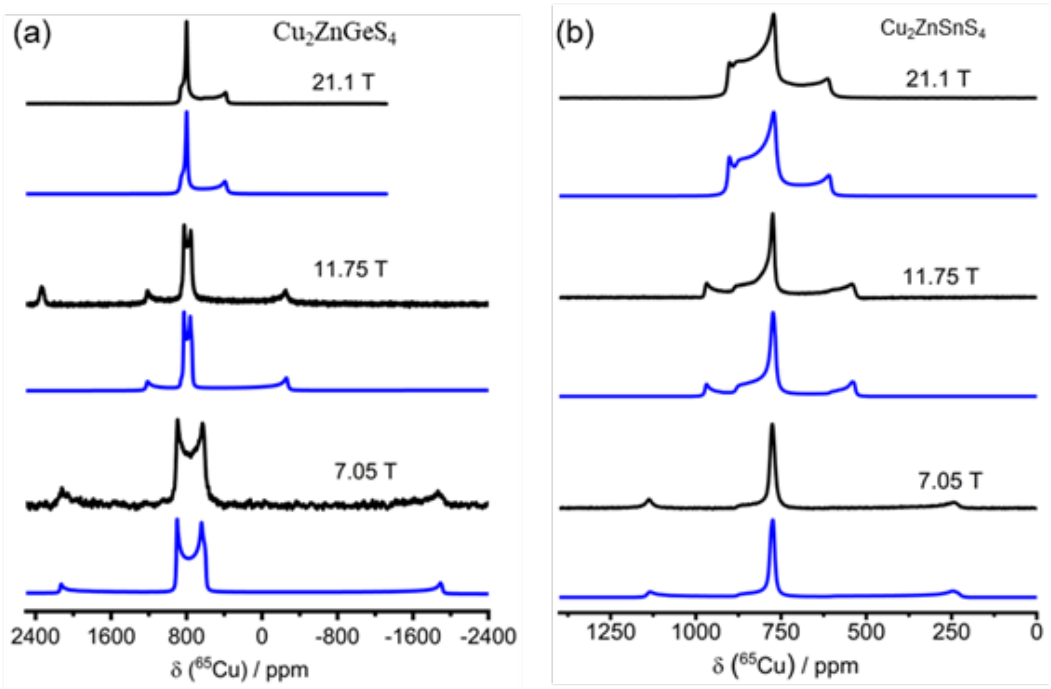

Figure S2. Experimental (black) and simulated (blue) ^{65}Cu NMR spectra of stationary samples at three applied magnetic fields for (a) Cu_2ZnGeS_4 and (b) Cu_2ZnSnS_4.

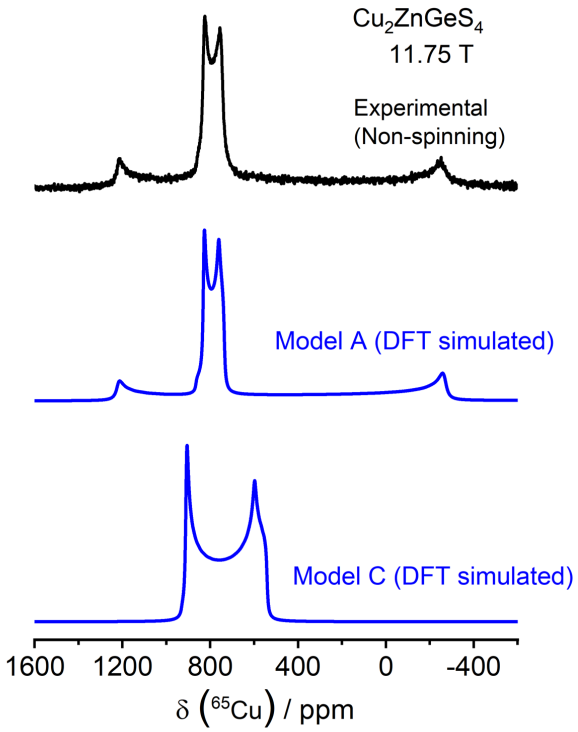

Figure S3. Experimental (black) and simulated (blue) ^{65}Cu NMR spectra of stationary samples for Cu_2ZnGeS_4 in models A and C. Parameters for the simulated spectra are listed in Table S5.

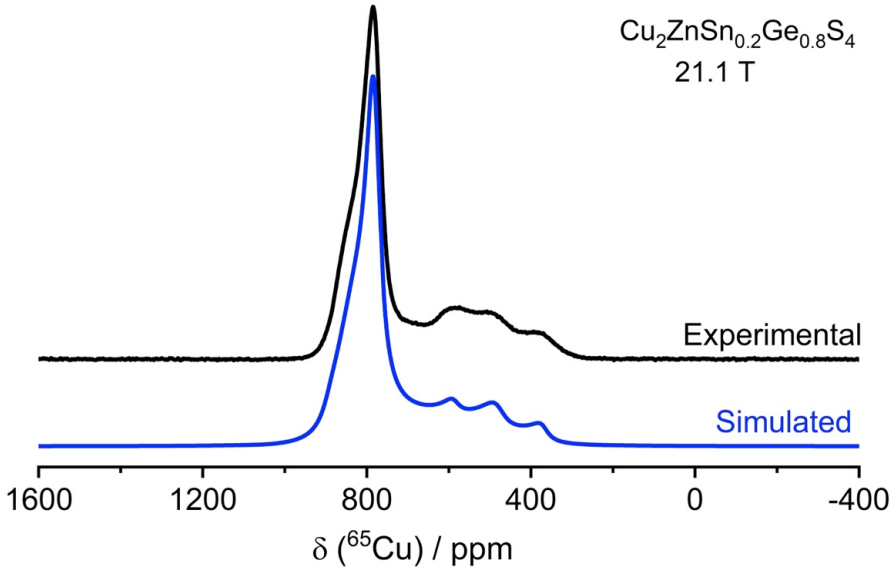

Figure S4. Experimental (black) and simulated (dark blue) ^{65}Cu NMR spectra of stationary samples for $Cu_2ZnSn_{0.2}Ge_{0.8}S_4$ in model A. Parameters for the simulated spectra are listed in Table S6.

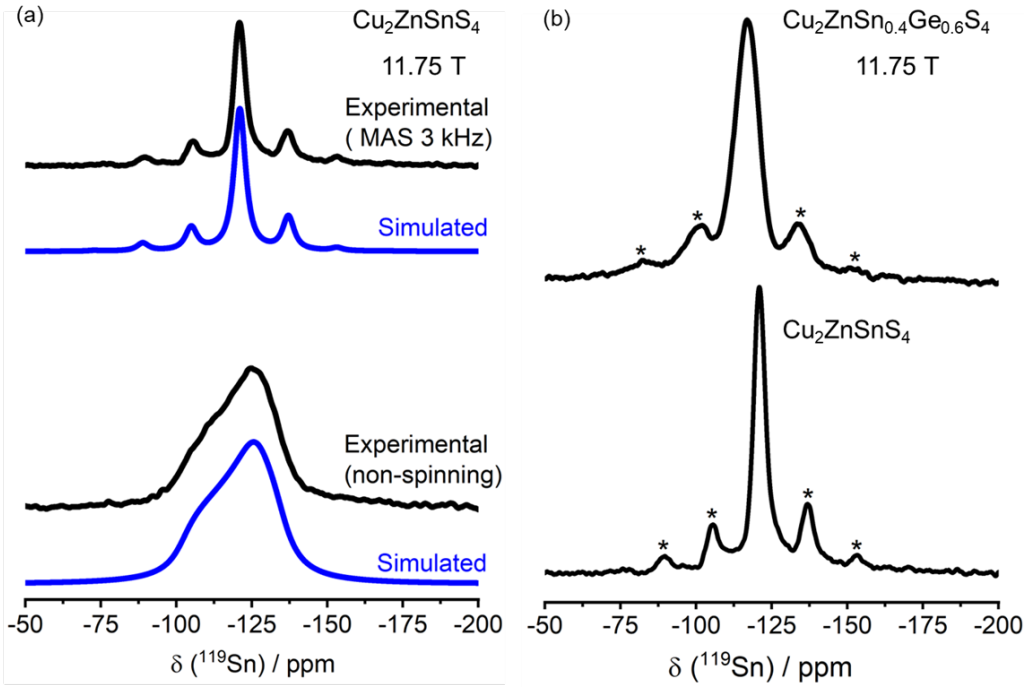

Figure S5. (a) Experimental (black) and simulated (blue) ^{119}Sn slow spinning ($\omega_r/2\pi$ = 3 kHz) and non-spinning NMR spectra for Cu_2ZnSnS_4 (B_0 = 11.75 T, δ_{iso} = −121 ppm, Ω = 32 ppm, and κ = 0.4). (b) Comparison of slow MAS ($\omega_r/2\pi$ = 3 kHz) ^{119}Sn spectra for Cu_2ZnSnS_4 and $Cu_2ZnSn_{0.4}Ge_{0.6}S_4$ at 11.75 T.

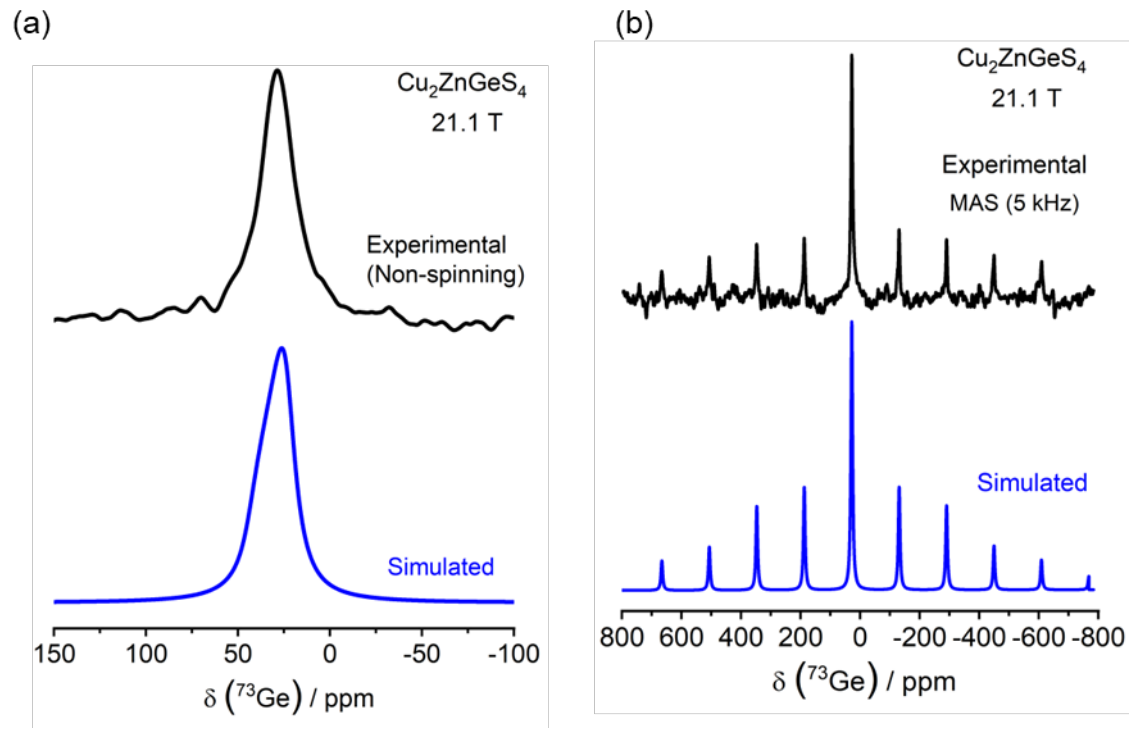

Figure S6. Experimental (black) and simulated (blue) (a) non-spinning and (b) ^{73}Ge MAS ($\omega_r/2\pi$ = 5 kHz) NMR spectra for Cu_2ZnGeS_4 (δ_{iso} = 28.5 ppm, C_Q = 0.3 MHz, η = 0) at 21.1 T.

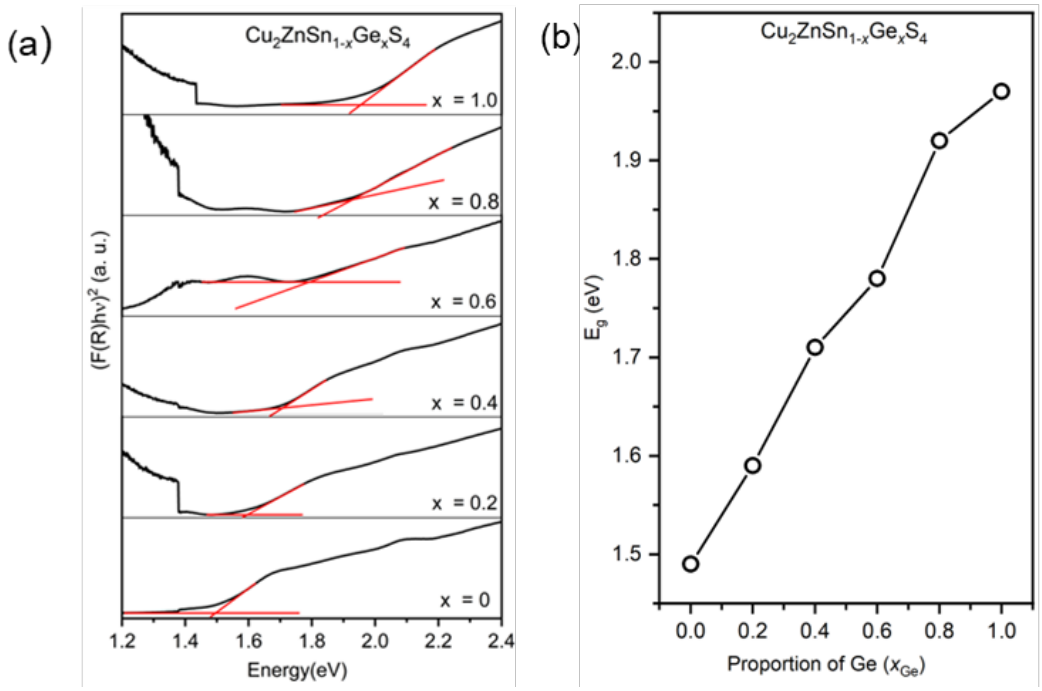

Figure S7. (a) Fittings of Tauc plots to extract optical band gaps. (b) Band gaps in $Cu_2ZnSn_{1-x}Ge_xS_4$.

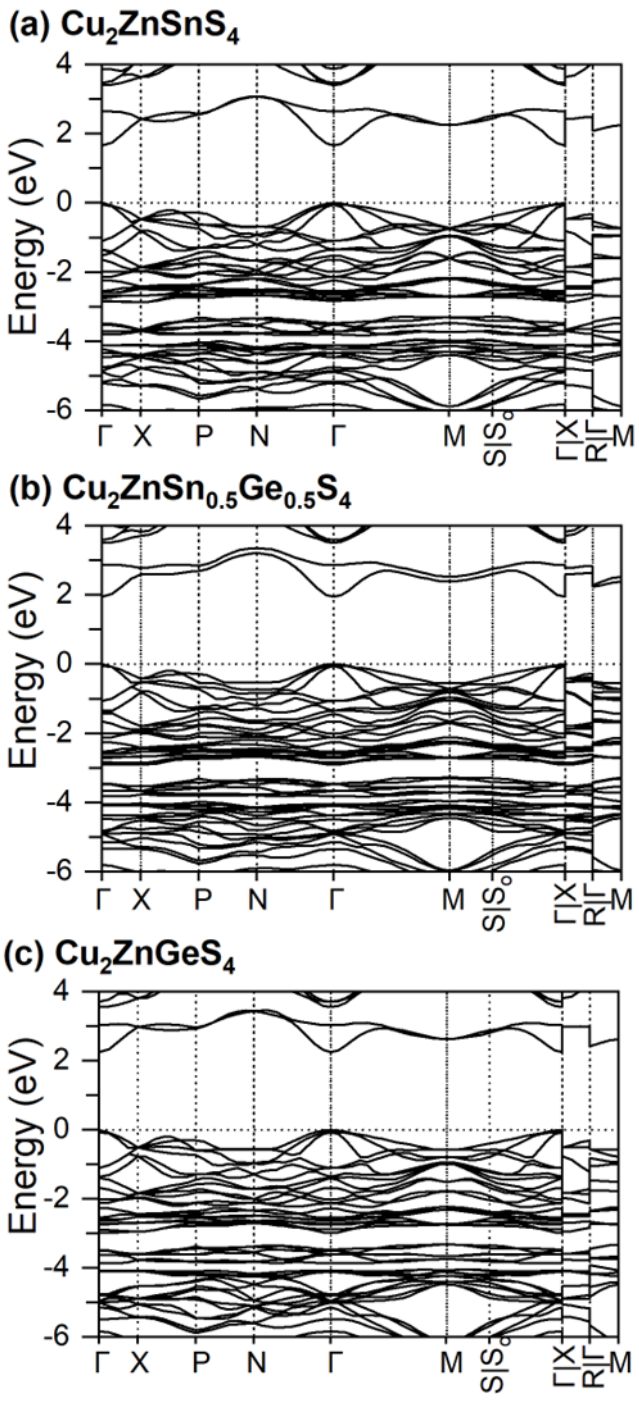

Figure S8. HSE06 band structure for (a) Cu_2ZnSnS_4, (b) $Cu_2ZnSnGeS_4$, and (c) Cu_2ZnGeS_4.

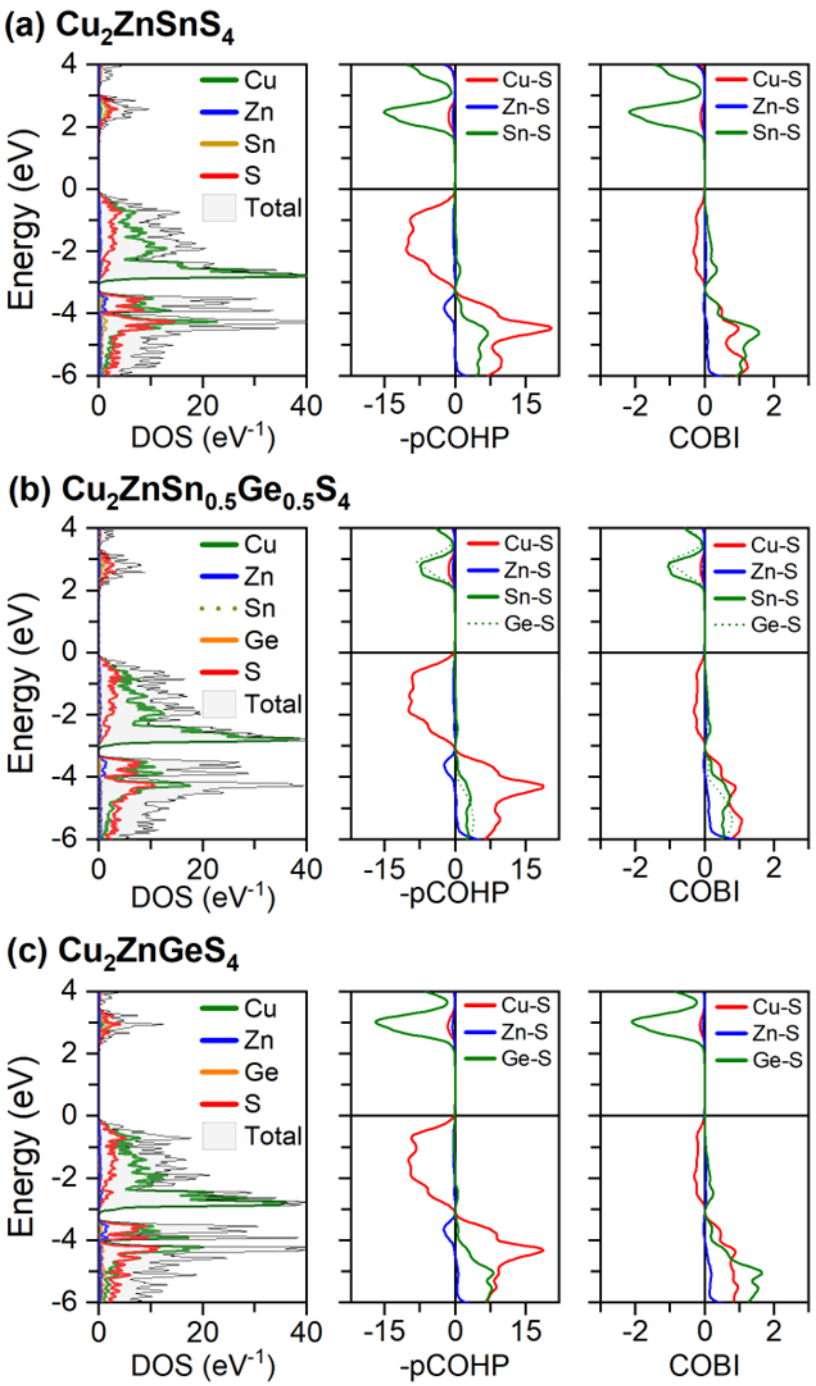

Figure S9. Density of states, crystal orbital Hamiltonian populations, and crystal orbital bond indices for (a) Cu_2ZnSnS_4, (b) $Cu_2ZnSnGeS_4$, and (c) Cu_2ZnGeS_4.